


ARTICLE OPEN



Smooth muscle 22 alpha protein inhibits VSMC foam cell formation by supporting normal LXR α signaling, ameliorating atherosclerosis

Dan-Dan Zhang^{1,5}, Yu Song^{1,5}, Peng Kong^{1,5}, Xin Xu¹, Ya-Kun Gao¹, Yong-Qing Dou², Lin Weng¹, Xiao-Wei Wang³, Yan-Ling Lin¹, Fan Zhang¹, Hailin Zhang⁴ and Mei Han¹ 

© The Author(s) 2021

Vascular smooth muscle cells (VSMCs) are indispensable components in foam cell formation in atherosclerosis. However, the mechanism behind foam cell formation of VSMCs has not been addressed. We found a potential association between deletion of smooth muscle (SM) 22 α and deregulated nuclear receptors liver X receptors (LXRs)/retinoid X receptor (RXR) signaling in mice. Here, we investigated the roles of SM22 α in LXR α -modulated cholesterol homeostasis, and explore possible mechanisms underlying this process. We identified that the depletion of SM22 α was a primary event driving VSMC cholesterol accumulation and the development of atherosclerosis in mice. Proteomic and lipidomic analysis validated that downregulation of SM22 α was correlated with reduced expression of LXR α and ATP-binding cassette transporter (ABCA) 1 and increased cholesteryl ester in phenotypically modulated VSMCs induced by platelets-derived growth factor (PDGF)-BB. Notably, LXR α was mainly distributed in the cytoplasm rather than the nucleus in the neointimal and Sm22 α ^{-/-} VSMCs. Loss of SM22 α inhibited the nuclear import of LXR α and reduced ABCA1-mediated cholesterol efflux via promoting depolymerization of actin stress fibers. Affinity purification and mass spectrometry (AP-MS) analysis, co-immunoprecipitation and GST pull-down assays, confocal microscopy, and stochastic optical reconstruction microscopy (STORM) revealed that globular-actin (G-actin), monomeric actin, interacted with and retained LXR α in the cytoplasm in PDGF-BB-treated and Sm22 α ^{-/-} VSMCs. This interaction blocked LXR α binding to Importin α , a karyopherin that mediates the trafficking of macromolecules across the nuclear envelope, and the resulting reduction of LXR α transcriptional activity. Increasing SM22 α expression restored nuclear localization of LXR α and removed cholesterol accumulation via inducing actin polymerization, ameliorating atherosclerosis. Our findings highlight that LXR α is a mechanosensitive nuclear receptor and that the nuclear import of LXR α maintained by the SM22 α -actin axis is a potential target for blockade of VSMC foam cell formation and development of anti-atherosclerosis.

Cell Death and Disease (2021)12:982; <https://doi.org/10.1038/s41419-021-04239-w>

INTRODUCTION

Vascular smooth muscle cells (VSMCs) are a major cell type present at intimal thickenings and all stages of an atherosclerotic plaque but with altered phenotypes [1]. The phenotypic switching of VSMCs, which is characterized by reduced myofilament density and contractile protein expression, is a key event during the development of atherosclerosis [2, 3]. Recently, the relative contribution of VSMCs to total foam cell formation has been determined in human atherosclerosis and in the model of mice [4, 5]. However, the mechanism underlying phenotypically switched VSMCs transforming into foam cells remains unclear.

Liver X receptors (LXRs) are members of the nuclear receptor superfamily of ligand-activated transcription factors and are primarily located in the nuclei with or without bound ligand and

regulate the expression of genes involved in cholesterol metabolism and inflammation in a tissue-specific manner [6, 7]. The intranuclear concentration of LXRs is maintained by a balance between nuclear import, nuclear export, and nuclear retention. The regulation of this balance provides important regulatory mechanisms for transcription [8]. LXR α -driven expression of the cholesterol efflux transporter ATP-binding cassette transporter (ABCA) 1 is essential for optimal reverse cholesterol transport in peripheral cells, which are associated with the pathogenesis of atherosclerosis [9]. VSMCs switched from contractile to synthetic phenotype metabolize lipids differently to contractile VSMCs, in part through decreased expression of ABCA1, resulting in an increased tendency to transform into foam cells [1, 6], but coordinated regulation of these processes has not been documented.

¹Department of Biochemistry and Molecular Biology, College of Basic Medicine, Key Laboratory of Medical Biotechnology of Hebei Province, Cardiovascular Medical Science Center, Hebei Medical University, Shijiazhuang, Hebei, P.R. China. ²College of Integrative Medicine, Hebei University of Chinese Medicine, Shijiazhuang, Hebei, P.R. China. ³Department of Laboratory of Lipid Metabolism, Institute of Basic Medicine, Hebei Medical University, Shijiazhuang, Hebei, P.R. China. ⁴Department of Pharmacology, College of Basic Medicine, Hebei Medical University, Shijiazhuang, Hebei, P.R. China. ⁵These authors contributed equally: Dan-Dan Zhang, Yu Song, Peng Kong. ✉email: hanmei@hebm.edu.cn

Edited by Professor Anastasis Stephanou

Received: 9 July 2021 Revised: 11 September 2021 Accepted: 29 September 2021

Published online: 22 October 2021

Smooth muscle (SM) 22 α (also known as Transgelin), a differentiated VSMC marker [10], is involved in actin filament assembly and cytoskeletal rearrangements [11], which is required for maintaining the differentiated phenotype of VSMCs [12, 13]. The expression of SM22 α has been demonstrated to be down-regulated in atherosclerosis and neointima, and further resulted in the depolymerization of the F-actin cytoskeleton, which represents phenotypic changes of VSMCs from the contractile to the synthetic [14, 15]. Loss of SM22 α in hypercholesterolemic *ApoE*-deficient mice results in increased atherosclerotic lesion area and a higher proportion of proliferating SMC-derived plaque cells [16], implying that there is a potential causal relationship between SM22 α depletion and atherosclerotic lesion. We and others have demonstrated that disruption of SM22 α enhances the inflammatory response in VSMCs [17–19]. Conversely, overexpression of SM22 α inhibits proliferation, inflammation, and oxidative stress of VSMC via blockade of different upstream pathways, and prevents neointima hyperplasia and aortic aneurysm formation [20–22]. Furthermore, these physiological and pathological effects of SM22 α are mediated by the regulation of actin dynamics to some extent [16, 17]. Recently, the aortic transcriptome profiling suggests that SM22 α knockout (*Sm22 α ^{-/-}*) mice exhibited the characteristics of pro-atherosclerosis with deregulated nuclear receptors LXR/RXR (retinoid X receptor) and atherosclerosis signaling pathways [20]. Thus, we hypothesized that the protective effects of SM22 α on vascular homeostasis may involve the regulation of LXR signaling.

In the current study, we first demonstrated that nuclear accumulation of LXRA is regulated by SM22 α -modulated actin dynamics, and altered actin dynamics by SM22 α depletion and the resulting inhibition of LXRA nuclear import accelerate the transformation of VSMCs into foam cells and development of atherosclerosis. Monomeric actin (G-actin) from F-actin depolymerization disturbs LXRA nuclear import and retains it in the cytoplasm. The normal LXRA signaling supported by SM22 α is a potential target for blockade of VSMC foam cell formation and development of anti-atherosclerosis.

RESULTS

Depletion of SM22 α contributes to the development of atherosclerosis in mice

We first took advantage of the published transcriptome analysis obtained on mouse aorta [23], to directly evaluate the sensitivity of *Sm22 α ^{-/-}* mice to atherosclerosis. The levels of serum total cholesterol (TC) and low-density lipoprotein cholesterol (LDL-C) gradually increased and were significantly higher in *Sm22 α ^{-/-}* mice than that in wild-type (WT) mice when fed the Paigen diet for 24 weeks with no change of serum triglyceride (TG) levels (Supplementary Fig. 1a–c). The diet significantly increased aortic cholesterol and cholesteryl ester (CE) content in *Sm22 α ^{-/-}* mice (Supplementary Fig. 1d). A positive oil red O staining was observed in aortic sinus sections of *Sm22 α ^{-/-}* but not of WT mice when fed the Paigen diet, accompanied with diffuse vascular wall thickening (Fig. 1a, b). Moreover, *Sm22 α ^{-/-}Ldlr^{-/-}* mice on a Paigen diet displayed an aggravated atherosclerotic lesion compared to *Ldlr^{-/-}* mice (Fig. 1a and Supplementary Fig. 1e), consistent with the previous finding [16].

Aortic stiffness is believed to be the earliest detectable manifestation of adverse structural and functional changes within the aortic wall [24]. Compared with WT mice, the aortic stiffness parameters, including elastic modulus, stiffness index, and reverse/forward flow ratio, were obviously increased in the outflow tract and aortic arch of *Sm22 α ^{-/-}* mice fed Paigen diet, while aortic distensibility was decreased significantly compared with WT mice (Fig. 1c and Supplementary Fig. 1f). HE staining for the aortic sections also showed incomplete vascular structure and fragmentation of elastic fiber (Supplementary Fig. 1e) and a notable

increase of fibrosis in the outflow tract and aortic arch of *Sm22 α ^{-/-}* mice fed Paigen diet for 12 weeks (Supplementary Fig. 1g, h), which was earlier than the atherosclerotic lesion. The expression of collagen I α (Col1 α) increased and elastin (Eln) decreased in the aortic tissues of *Sm22 α ^{-/-}* mice (Supplementary Fig. 1i), suggesting that *Sm22 α ^{-/-}* mice develop an aortic stiffness phenotype.

Bodipy staining showed that $50 \pm 2\%$ of foam cells costained strongly with smooth muscle marker α -actin (ACTA2) (Fig. 1d). Cells expressing both ACTA2 and CD68 that is a marker for macrophages as a percentage of total CD68⁺ cells were $12 \pm 2\%$ ($n = 6$) in the atherosclerotic lesions of *Sm22 α ^{-/-}* mice (Fig. 1d), which was approximately one-fourth of the macrophages, consistent with that observed in the atherosclerotic lesions of *ApoE^{-/-}* mice and human coronary artery [5]. The expression of LXRA and ABCA1 at mRNA and protein levels decreased in the aortic tissues from *Sm22 α ^{-/-}* mice fed with Paigen diet or not, compared with WT mice (Supplementary Fig. 1j, k). Surprisingly, we observed numerous nuclear LXRA-staining negative VSMCs in the aortic sections from *Sm22 α ^{-/-}* mice (Fig. 1e), suggesting that LXRA nuclear localization is disturbed. Overall, these data demonstrated that SM22 α depletion induces arteriosclerosis via a mechanism that involves the dysfunction of LXRA activity.

Expression and activity of LXRA are abnormal in *Sm22 α ^{-/-}* VSMCs

We next mainly examined the effect of SM22 α loss on the expression and distribution of LXRs in VSMCs as macrophages did not express SM22 α [25]. The expression of LXRA was lower in *Sm22 α ^{-/-}* VSMCs than that in WT cells under basic conditions, and no difference in LXRB expression was observed. T090- and cholesterol-induced LXRA expression was repressed in *Sm22 α ^{-/-}* VSMCs compared to WT VSMCs (Fig. 2a and Supplementary Fig. 2a). To further establish the causal relevance of SM22 α in the expression of LXRA, WT VSMCs were transfected with the specific siRNA of SM22 α and *Sm22 α ^{-/-}* VSMCs with Ad-GFP-SM22 α . We showed that knockdown of SM22 α resulted in reduced expression of LXRA at mRNA and protein levels in WT VSMCs with or without cholesterol loading (Fig. 2b). Conversely, the downregulation of LXRA was significantly reversed by the rescue of SM22 α expression in *Sm22 α ^{-/-}* VSMCs (Fig. 2c).

As VSMCs with negative nuclear LXRA-staining were found in the aortic sections of *Sm22 α ^{-/-}* mice, we next determined whether the subcellular distribution of LXRA is changed in *Sm22 α ^{-/-}* VSMCs. We showed that endogenous LXRA was mainly accumulated in the nucleus of WT VSMCs. However, nuclear LXRA was almost little in *Sm22 α ^{-/-}* VSMCs, which exhibited diffuse cytoplasmic staining (Fig. 2d), and the ratio of cytoplasmic-/nuclear-LXRA protein markedly increased compared to WT controls (Supplementary Fig. 2b). The rescue of SM22 α expression restored endogenous LXRA nuclear localization in *Sm22 α ^{-/-}* VSMCs (Fig. 2e), whereas the overexpression of LXRA-GFP was unable to do this, suggesting that LXRA nuclear accumulation is SM22 α -dependent and not influenced by LXRA level, and that defect of LXRA nuclear localization further reduces its expression, as LXRA is also a direct target gene of LXRA and enhances its own expression [26].

Activation of LXRA is also able to suppress collagen expression not only promotes transcription of lipid transport and, metabolism genes [27, 28], and VSMCs, as the main origin of extracellular matrix (ECM), are a significant regulator of ECM remodeling and arterial stiffness [29]. We showed that the mRNA level of ABCA1, ABCG1, and Eln was significantly downregulated (Fig. 2f), while the expression of Col1 α was significantly elevated in *Sm22 α ^{-/-}* VSMCs under basic and cholesterol loading conditions. By comparison, SM22 α loss had little effect on the expression of cholesterol intake genes LDL receptor (LDLR) and scavenger receptor class B type I (SR-BI). Cholesterol-induced dynamic upregulation of ABCA1 expression observed from WT cells was missed in *Sm22 α ^{-/-}* VSMCs (Fig. 2g), accompanied by increased cholesterol accumulation in a time-dependent manner (Fig. 2h). Reduced ABCA1

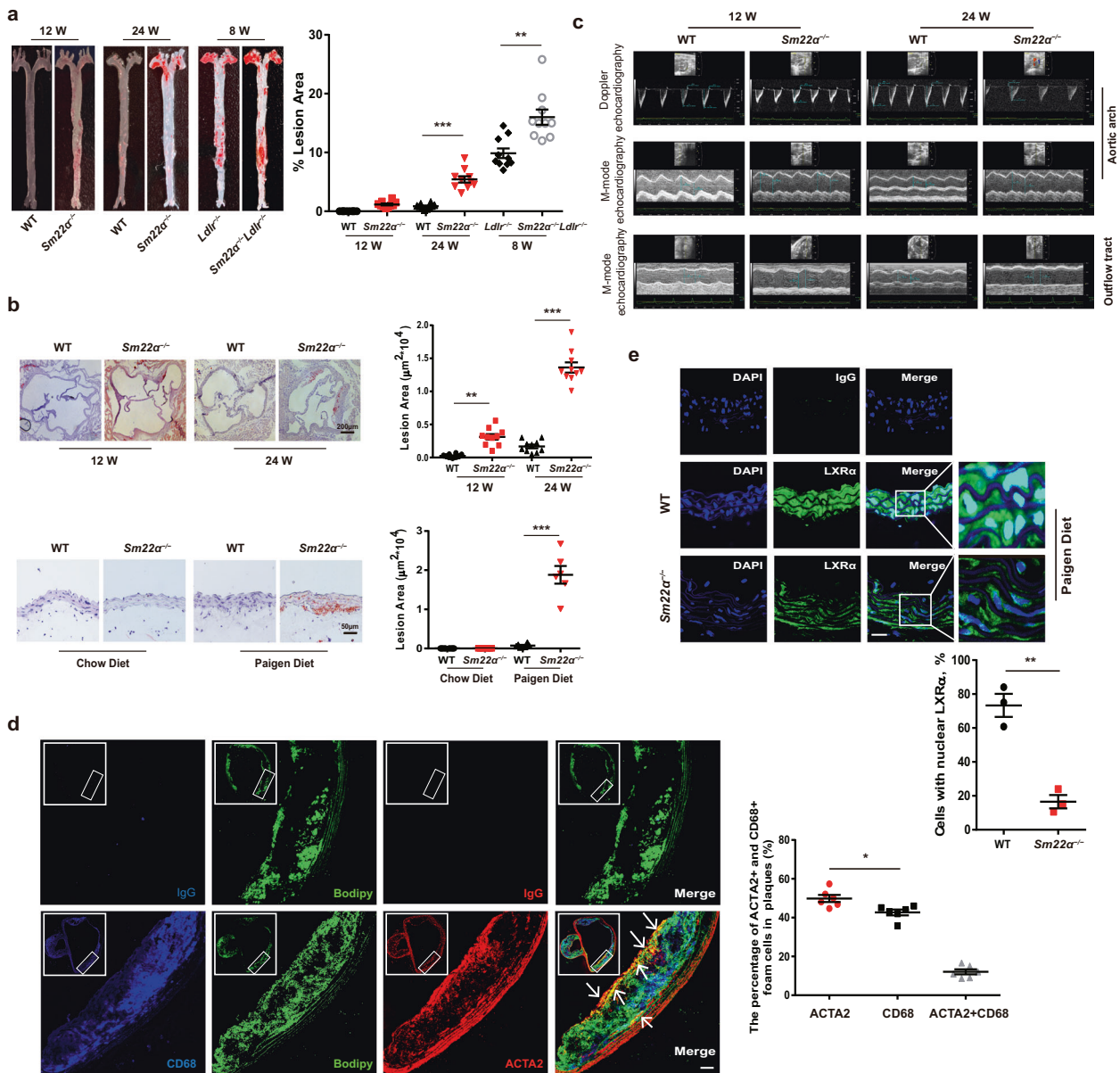
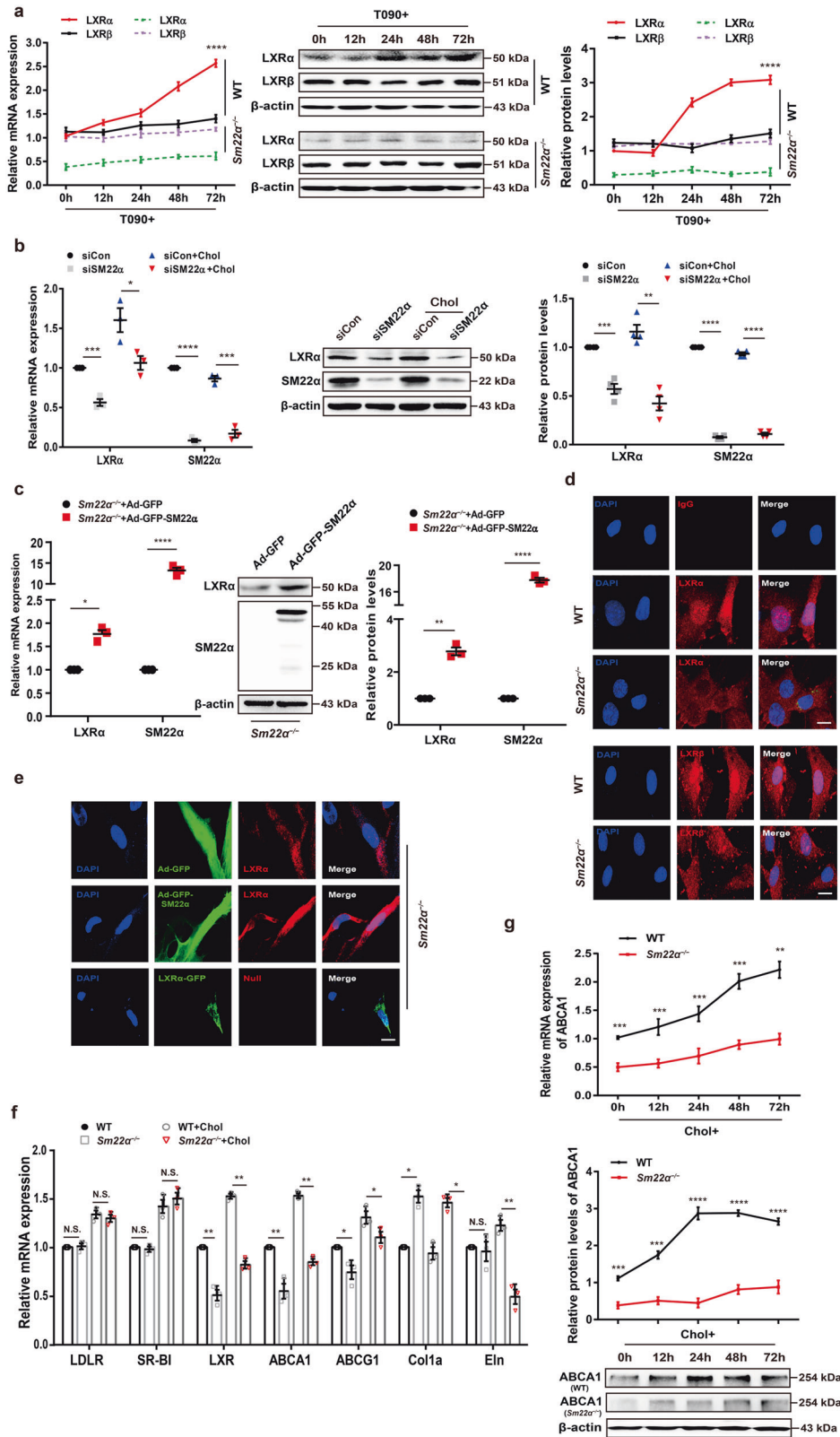


Fig. 1 Impaired SM22 α expression is associated with the development of atherosclerosis. **a**, **b** WT ($n = 10$) and $Sm22\alpha^{-/-}$ ($n = 10$) mice with or without $Ldlr^{-/-}$ background ($n = 10$) fed Paigen diet for 8, 12 and 24 weeks respectively. Representative images of en face ORO-stained aortas (**a**), aortic sinus, aortic cross-sections (**b**) and quantification of lesion areas are shown. **c** M-mode and Doppler echocardiography images obtained from the aortic arch and outflow tract of WT ($n = 15$) and $Sm22\alpha^{-/-}$ ($n = 15$) mice fed Paigen diet for 12 and 24 weeks. A_s : outflow tract and aortic diameter in systole; A_d : outflow tract and aortic diameter in diastole. **d** Identification of SMC-derived foam cells within atherosclerotic lesion of $Sm22\alpha^{-/-}$ mice ($n = 6$) by CD68 (blue), ACTA2 (red) and Bodipy (green). Scale bar, 20 μ m. Arrows indicated foam cells that were VSMCs-derived. **e** Representative immunofluorescence of LXR α (red) and quantification of cells with nuclear LXR α in the aortic sections from WT ($n = 3$) and $Sm22\alpha^{-/-}$ ($n = 3$) mice. Scale bar, 15 μ m. Data and images are representative of at least three independent experiments. Data in (**a**) and (**b**) were analyzed by two-way and one-way ANOVA respectively. Data in (**d**) and (**e**) were analyzed by unpaired t test. * $p < 0.05$; ** $p < 0.01$; *** $p < 0.001$.

expression and increased cholesterol accumulation were verified in VSMCs with knockdown of SM22 α (Supplementary Fig. 2c–e). Chromatin immunoprecipitation (ChIP) assay showed that the binding activity of LXR α to the promoter of *abca1* and *col1a* genes was decreased in $Sm22\alpha^{-/-}$ VSMCs compared to WT VSMCs (Fig. 2i, j), in accordance with decreased ABCA1 and increased Col1a expression. Rescue of SM22 α expression in $Sm22\alpha^{-/-}$ VSMCs by transduction with Ad-GFP-SM22 α increased in binding activity of LXR α to *col1a* promoter with a reduced Col1a expression (Supplementary Fig. 2f, g). Overall, these data indicate that LXR α transcriptional regulatory activity is repressed in $Sm22\alpha^{-/-}$ VSMCs.

Not only does cholesterol deposits in foam cells at the atherosclerotic plaque, it also regulates cellular mechanics in atherosclerosis progression [30]. Next, the force-curve and Young's modulus of individual VSMCs were measured by atomic force microscopy (AFM). E-modulus of $Sm22\alpha^{-/-}$ VSMCs was higher and significantly increased in response to cholesterol loading compared with WT cells (Fig. 2k), suggesting that cholesterol accumulation and substrate stiffness induce alternation of the biomechanics of VSMCs. Taken together, these results suggest that SM22 α loss contributes to stiffness and foam cell formation of VSMCs.



Nuclear localization and signaling of LXR α are impaired in phenotypically switched VSMCs

SM22 α loss is a prominent marker of phenotypic switching of VSMCs [10], and Sm22 α ^{-/-} VSMCs have the characteristic of synthetic and pro-inflammatory phenotypes [17–19]. To determine

whether the dysfunction of the LXR α -ABCA1 axis is common in phenotypically modulated VSMCs, we performed the proteomic analysis of the contractile and synthetic VSMCs and showed that the expression of ABCA1 was markedly reduced in the synthetic VSMCs (Fig. 3a, b and Supplementary Fig. 3a). We validated that

Fig. 2 Expression and activity of LXR α is abnormal in *Sm22 α ^{-/-}* VSMCs. **a** qRT-PCR and Western blot analysis of LXR α and LXR β in WT and *Sm22 α ^{-/-}* VSMCs treated with LXRs agonist T090 for 0, 12, 24, 48 and 72 h respectively ($n = 3$). **b** qRT-PCR and Western blot analysis of LXR α in WT VSMCs with or without cholesterol loading following knockdown of SM22 α ($n = 3$). **c** qRT-PCR and Western blot analysis of LXR α and SM22 α expression in *Sm22 α ^{-/-}* VSMCs transfected with Ad-GFP and Ad-GFP-SM22 α for 24 h ($n = 3$). **d** Confocal microscopy images of LXR α and LXR β distribution in WT and *Sm22 α ^{-/-}* VSMCs. Scale bar, 10 μ m. **e** Immunofluorescence staining for endogenous LXR α and LXR α -GFP in *Sm22 α ^{-/-}* VSMCs transfected with Ad-GFP and Ad-GFP-SM22 α or not. Scale bar, 10 μ m. **f** qRT-PCR analysis of cholesterol intake (LDLR, SR-BI), efflux genes (ABCA1, ABCG1), and sclerosis-related genes (Col1 α , Eln) in WT and *Sm22 α ^{-/-}* VSMCs incubated with or without cholesterol ($n = 3$). **g** The mRNA and protein levels of ABCA1 in WT and *Sm22 α ^{-/-}* VSMCs treated with cholesterol for 0, 12, 24, 48, and 72 h respectively ($n = 3$). **h** ORO staining of WT and *Sm22 α ^{-/-}* VSMCs stimulated with cholesterol for 0, 24, 48, and 72 h respectively and quantification of positive ORO staining. Scale bar, 20 μ m. **i** The binding activity of LXR α to the promoter of *abca1* gene was decreased in *Sm22 α ^{-/-}* VSMCs ($n = 4$). **j** ChIP and RT-PCR detected LXR α binding to *col1 α* promoter in WT and *Sm22 α ^{-/-}* VSMCs ($n = 6$). **k** The Young's modulus of WT and *Sm22 α ^{-/-}* VSMCs treated with or without cholesterol ($n = 120$). Data and images are representative of at least three independent experiments. Data in (a), (g), and (h) were analyzed by Kruskal–Wallis rank-sum test and two-way ANOVA. Data in (b), (c), (f), (i), and (j) were analyzed by unpaired *t* test. NS not significantly different; * $p < 0.05$; ** $p < 0.01$; *** $p < 0.001$; **** $p < 0.0001$.

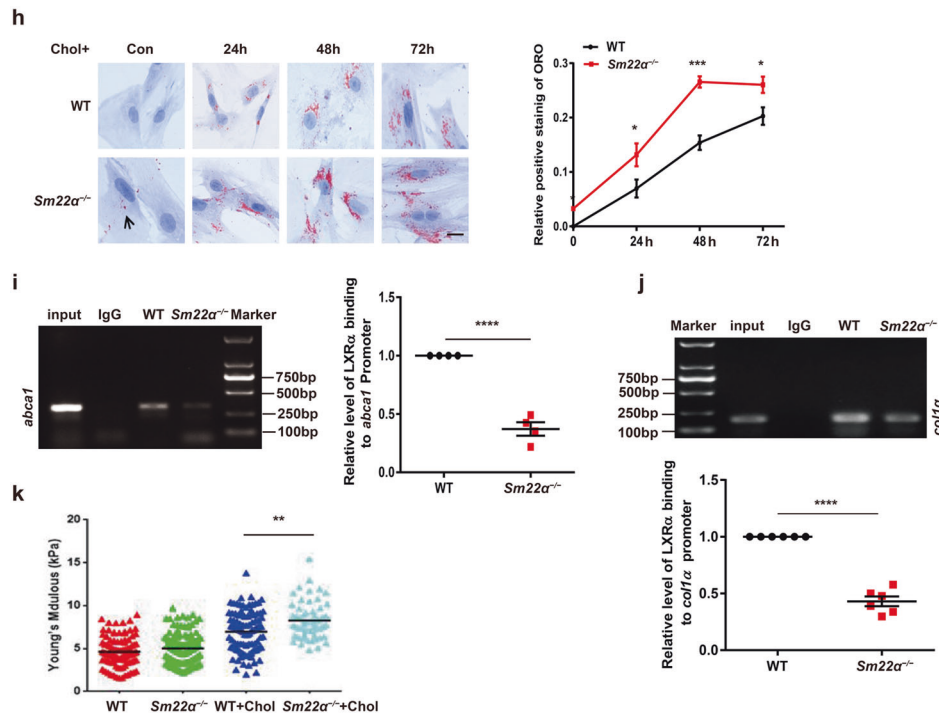


Fig. 3 Function of the LXR α -ABCA1 axis is impaired in phenotypically switched VSMCs. **a** Heatmap of proteomic analysis between synthetic and contractile VSMCs. **b** Analysis of KEGG pathway enriched by differentially expressed genes of proteomic analysis between synthetic and contractile VSMCs. **c** The mRNA expression of SM22 α , LXR α , and ABCA1 in WT VSMCs treated with PDGF-BB for 0, 12, 24, and 48 h respectively ($n = 3$). **d** Confocal microscopy images of LXR α distribution in WT VSMCs incubated with PDGF-BB for 0, 12, 24, and 48 h respectively. Scale bar, 10 μ m. **e** Confocal microscopy images of LXR α and ACTA2 in arterial walls of WT mice after ligation for 0, 7, 14, and 28 days. Scale bar, 20 μ m. **f** Quantification of each lipid class in synthetic and contractile VSMCs. Lipid classes were expressed as μ mol per g protein. **g** Heatmap of CEs between synthetic and contractile VSMCs. **h** ORO staining of WT VSMCs transfected with or without Ad-GFP-SM22 α following with PDGF-BB and/or cholesterol treatment and quantification of positive ORO staining. Scale bar, 20 μ m ($n = 3$). **i** M-mode and Doppler echocardiography images obtained from aortic arch and outflow tract of *Sm22 α ^{-/-}* mice transfected with AAV-GFP ($n = 10$) and AAV-SM22 α ($n = 10$) fed Paigen diet for 12 weeks. A_s : outflow tract and aortic diameter in systole; A_d : outflow tract and aortic diameter in diastole. **j** Representative images of en face ORO-stained aortas and quantification of lesion areas ($n = 6$). **k** Representative immunofluorescence of LXR α (green) and quantification of cells with nuclear LXR α in the aortic sections from *Sm22 α ^{-/-}* mice transfected with AAV-GFP ($n = 4$) and AAV-SM22 α ($n = 4$) fed Paigen diet for 24 weeks. Scale bar, 10 μ m. Arrows indicated the distribution of LXR α . **l** Identification of SMC-derived foam cells within atherosclerotic lesion of *Sm22 α ^{-/-}* mice infected with AAV-GFP ($n = 4$) and AAV-SM22 α ($n = 4$) fed Paigen diet for 24 weeks by CD68 (blue), ACTA2 (red) and Bodipy (green). Scale bar, 25 μ m. Arrows indicated foam cells that were VSMCs-derived. Data and images are representative of at least three independent experiments. Data in (c) were analyzed by two-way ANOVA. Data in (f), (h), (j), (k) and (l) were analyzed by unpaired *t* test. * $p < 0.05$; ** $p < 0.01$; *** $p < 0.001$; **** $p < 0.0001$.

the expression of SM22 α , ABCA1 and LXR α mRNAs decreased in a time-dependent manner in PDGF-BB-induced VSMCs (Fig. 3c). Notably, LXR α was gradually shifted from the nuclear to the cytoplasm in some VSMCs with extended PDGF-BB stimulation time (Fig. 3d). To determine whether nuclear localization of LXR α is impaired in modulated VSMCs in vivo, we examined VSMCs in the media and the neointima of mice. As expected, LXR α was mainly

distributed in the nucleus of the medial VSMCs in the normal artery, whereas LXR α localization was shifted from the nucleus to the cytoplasm and merged with ACTA2 in the neointima VSMCs undergoing phenotypic modulation (Fig. 3e), indicating that LXR α nuclear localization was disturbed in these modulated VSMCs. To further confirm the effect of reduced LXR α -ABCA1 activity on lipid metabolism, the lipid profiles of VSMCs treated with PDGF-BB were

assessed by a lipidomic analysis. Comparison of the lipidome between the contractile and synthetic phenotypes showed that CE was significantly increased compared with other lipids (Fig. 3f and Supplementary Fig. 3b), which was a prominent feature of the lipid profiles of synthetic VSMCs (Fig. 3g). Moreover, increased cholesterol deposition was also validated in PDGF-BB-induced VSMCs by ORO staining (Fig. 3h). Overall, these data further suggest that nuclear localization and signaling of LXRA are impaired during phenotypic switching of VSMCs, associated with the depletion of SM22a.

Targeting SM22a supports normal LXRA signaling and ameliorates atherosclerosis

To further identify a potential causative link between SM22a expression and LXRA signaling, we selected an AAV carrying SM22a to perform a gain-of-function study in *Sm22a*^{-/-} mice fed Paigen diet. As expected, the administration of AAV-SM22a restored SM22a expression in the aortic wall of *Sm22a*^{-/-} mice accompanied with enhanced aortic GFP signal, indicating a high efficiency of viral transfection (Supplementary Fig. 3c, e). Compared with AAV-GFP mice, the administration of AAV-SM22a significantly reduced Paigen diet-induced aortic stiffness and atherosclerotic lesion (Fig. 3i, j and Supplementary Fig. 3d, e), indicating that AAV-SM22a intervention is effective. qRT-PCR showed that Col1a expression was decreased and the expression of Eln, LXRA and ABCA1 was elevated in the aortic wall of *Sm22a*^{-/-} mice with AAV-SM22a (Supplementary Fig. 3f), accompanied with reduced expression of MCP-1, MMP2, MMP9, VCAM-1 and ICAM-1 that are downstream of NF-κB, as LXRA has been reported to inhibit NF-κB activity [31]. Importantly, LXRA was mainly accumulated in the nucleus of VSMCs (Fig. 3k), and VSMC marker positive foam cells were reduced in the aortic arch of *Sm22a*^{-/-} mice with AAV-SM22a (Fig. 3l). Collectively, these findings suggest that SM22a ameliorates atherosclerosis via supporting nuclear localization of LXRA.

Nuclear import of LXRA is regulated by actin dynamics

To elucidate the mechanism underlying cytoplasmic retention of LXRA, nuclear import of LXRA-GFP was measured by fluorescence loss in photobleaching (FLIP) and fluorescence recovery after photobleaching (FRAP) experiments. In WT cells, nuclear import of LXRA-GFP was extremely rapid, being effectively complete within 2 min (Fig. 4a and Supplementary Movie 1) and dramatically delayed and reduced in *Sm22a*^{-/-} cells (Supplementary Movie 2). LXRA phosphorylation and the formation of a heterodimer with retinoid X receptor (RXR) have been demonstrated to be required for LXRA nuclear accumulation [32, 33]. We showed that SM22a loss did not affect the phosphorylation of LXRA (Supplementary Fig. 4a), and also had no effect on the interaction between LXRA and RXR (Supplementary Fig. 4b).

To investigate the possible sequestering proteins that retard LXRA nuclear import, we performed affinity purification using an anti-LXRA antibody, and the precipitates were subjected to mass spectrometry analysis. A total of 48 proteins potentially interacting with LXRA was identified (Supplementary Table). Next, we used GO enrichment analysis to cluster and characterize these proteins according to their biological processes (Supplementary Fig. 4c). Ultimately, the actin associated with muscle cell differentiation was selected as a candidate for its reported function in guiding transcriptional factors nuclear transport [34, 35]. As disruption of SM22a promotes actin cytoskeleton remodeling in VSMCs [17, 22], we subsequently compared actin organization between *Sm22a*^{-/-} and WT cells. *Sm22a*^{-/-} VSMCs exhibited less fraction of bundled stress fibers (Fig. 4b), and a higher total G-actin and parallel reduced ratio of F-actin to G-actin compared to WT cells (Supplementary Fig. 4d). Moreover, LXRA was mainly distributed in the perinuclear area of the cytoplasm with less F-actin in *Sm22a*^{-/-} VSMCs (Fig. 4c). To validate whether altered actin

organization is associated with impaired nuclear translocation of LXRA, VSMCs were treated with jasplakinolide (JPK) which stabilizes F-actin and cytochalasin-B (CytoB) that inhibits actin polymerization. We showed that LXRA almost entirely remained in the cytoplasm of VSMCs treated by CytoB (Fig. 4d), with a decreased ratio of F-actin to G-actin (Supplementary Fig. 4d), and JPK did not affect the nuclear accumulation of LXRA. CytoB washout restored actin dynamics and distribution of LXRA in the nucleus (Fig. 4d and Supplementary Fig. 4d). Western blot for LXRA expression in the nuclear and cytoplasm fractions showed that LXRA protein was gradually shifted from the nuclear to the cytoplasm during CytoB treatment for different times, with increased cytoplasm/nucleus ratio of LXRA (Fig. 4e). Together, these data for the first time demonstrated that LXRA is a mechanosensitive nuclear receptor and that nuclear translocation of LXRA is regulated by actin dynamics.

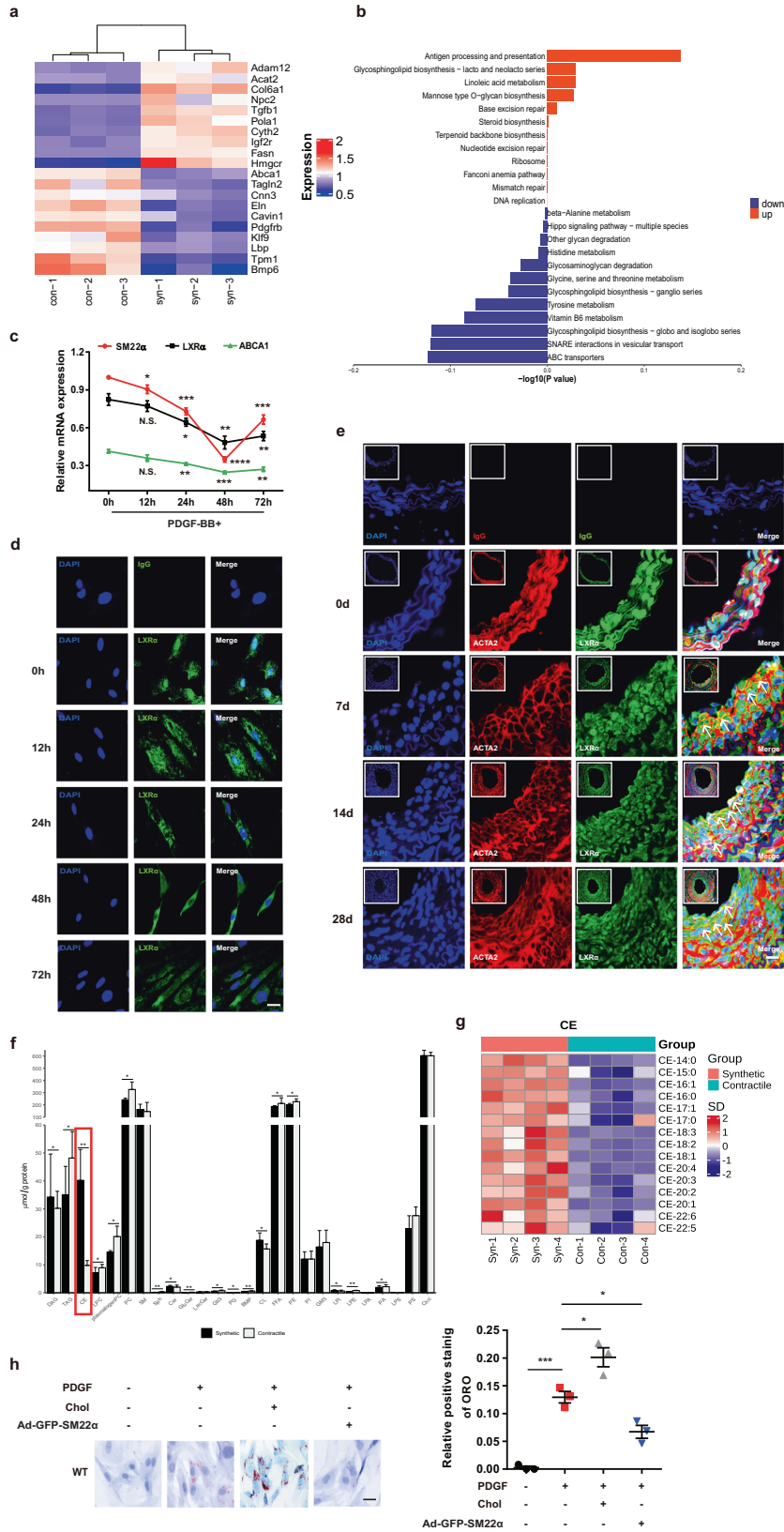
G-actin directly interacts with and retains LXRA in the cytoplasm

To test whether LXRA directly interacts with actin *in vivo*, we performed computational docking analysis for G-actin and LXRA via the ZDOCK server and discovered the highest-scored predicted model of interaction between them (Supplementary Fig. 4e). As LXRA did not colocalize with the F-actin cytoskeleton (Fig. 4c), we used Dnasel to label G-actin and observed that G-actin colocalized with LXRA in the cytoplasm of *Sm22a*^{-/-} and CytoB-treated VSMCs (Fig. 5a). Next, F-actin and G-actin fractions isolated from WT and *Sm22a*^{-/-} VSMCs were subjected to co-immunoprecipitation (co-IP) with specific anti-ACTA2 and anti-LXRA antibodies. A specific LXRA band was present in the complex immunoprecipitated by the anti-ACTA2 antibody in the G-actin fraction but not in the F-actin fraction of *Sm22a*^{-/-} but not WT VSMCs (Fig. 5b). Meanwhile, ACTA2 did not co-immunoprecipitate with LXRA in both F-actin and G-actin fractions of *Sm22a*^{-/-} VSMCs (Fig. 5c). Importantly, an atherosclerotic lesion assay using DNaseI and anti-LXRA antibodies revealed a colocalization between endogenous LXRA and G-actin in the aortic wall of *Sm22a*^{-/-} mice (Fig. 5d). To further validate that increased G-actin level contributes to the retention of LXRA in the cytoplasm, we overexpressed HA-ACTA2 in WT VSMCs and showed that DNaseI-stained G-actin markedly increased (Supplementary Fig. 5a). Importantly, endogenous LXRA redistributed from the nucleus to the cytoplasm and colocalized with ACTA2 in the VSMCs (Fig. 5e), and exogenous LXRA-GFP was so in co-expressed cells. Similar results were observed in HEK-293A cells co-expressing LXRA-GFP and HA-ACTA2, different from the cells expressing LXRA-GFP alone that had nuclear LXRA-GFP fluorescence (Fig. 5f). Thus, G-actin is a novel inhibitor of LXRA nuclear accumulation.

To gain direct insight into G-actin-LXRA interaction in cells, we exploited stochastic optical reconstruction microscopy (STORM) [36], a super-resolution imaging method, to examine the spatial distributions of the two proteins. In WT cells, an obvious much broader peak was observed for the nearest-neighbor distribution of LXRA and G-actin (Fig. 5g). Upon treatment with CytoB, STORM displayed a significant reduction in the nearest-neighbor distance between LXRA and G-actin (Fig. 5h). A quantitatively similar increase in colocalization between LXRA and G-actin was observed using *Sm22a*^{-/-} VSMCs (Fig. 5i). Such colocalization was abolished by the rescue of SM22a expression (Fig. 5j). Together, these findings suggest that LXRA is recruited by G-actin.

G-actin binding disturbs interaction between LXRA and Importin α

Binding to Importin α that is to serve as an adaptor is the first step in the nuclear transport of nuclear receptors by that link them to Importin β to form a ternary complex in the cytoplasm [37]. We observed that neither CytoB treatment nor loss of SM22a changed Importin α expression (Fig. 5k). Notably, the expression of Importin



α in the LXR α -immunoprecipitated complex decreased evidently or even disappeared in *Sm22a*^{-/-} VSMCs compared to WT cells, which was returned the level to WT cells via the rescue of SM22 α expression (Fig. 5k). Similarly, the LXR α -Importin α complex was

decreased in CytoB and PDGF-BB-treated WT VSMCs, accompanied with reduced nuclear LXR α expression (Supplementary Fig. 5b), indicating that Importin α -mediated LXR α nuclear import was inhibited by altered actin dynamics, associated with VSMC

Fig. 4 Nuclear import of LXR α is regulated by actin dynamics. **a** Fluorescence recovery after photobleaching (FRAP) studies with LXR α -GFP to measure nuclear import. Cells were pretreated with LMB. Decreased accumulation of nuclear fluorescence indicates a lower rate of nuclear import of LXR α -GFP in *Sm22a*^{-/-} VSMCs relative to WT controls ($n = 25$). **b** Representative images of F-actin (phalloidin, red) and G-actin (Dnase1, green) in WT and *Sm22a*^{-/-} VSMCs. Scale bar, 10 μ m. **c, d** Representative images for F-actin (phalloidin, red) and LXR α (green) in WT and *Sm22a*^{-/-} VSMCs with cholesterol loading or not (**c**) and in WT VSMCs treated with JPK, CytoB and after CytoB washout (**d**). Scale bars, 10 μ m. **e** Western blot analysis of cytoplasmic and nuclear LXR α in WT VSMCs treated with CytoB at different time points ($n = 6$). Data and images represent at least three independent experiments. Statistical analyses, unpaired t test and Kruskal–Wallis rank-sum test. ** $p < 0.01$; **** $p < 0.0001$.

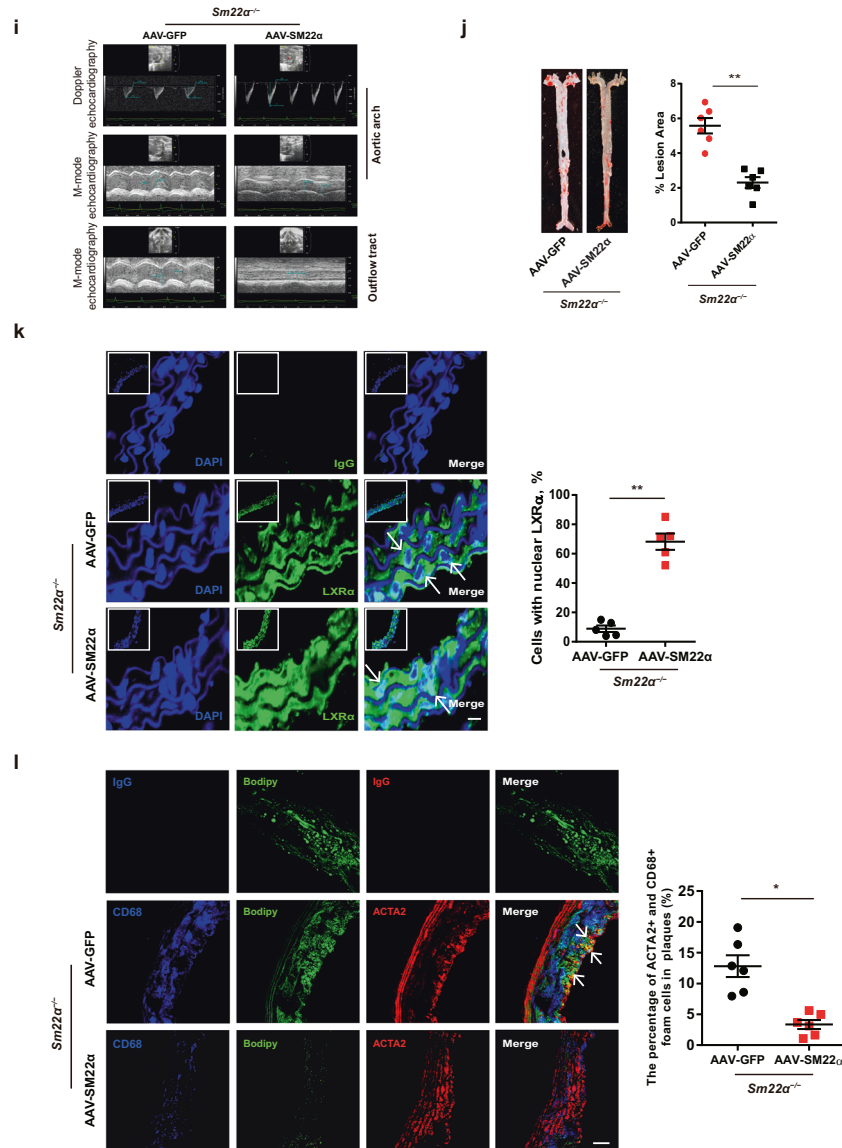


Fig. 5 G-actin interacts with and retains LXR α in the cytoplasm, blocking LXR α binding to Importin α . **a** Double immunofluorescence staining for G-actin (Dnase1, red) and LXR α (green) in WT VSMCs accompanied with the treatment of JPK or CytoB and also in *Sm22a*^{-/-} VSMCs. Scale bar, 10 μ m. **b, c** Co-immunoprecipitation of ACTA2 and LXR α (**b**) and LXR β (**c**) respectively in F- and G-actin fractions of WT and *Sm22a*^{-/-} VSMCs ($n = 3$). **d** Double immunofluorescence staining of G-actin (Dnase1, red) and LXR α (green) or IgG in the atherosclerotic lesion in the aortic wall of *Sm22a*^{-/-} mice. Scale bar, 20 μ m. **e** Representative immunofluorescence staining for endogenous LXR α (green) and LXR α -GFP (green) in WT VSMCs transfected with HA-ACTA2 (red, stained by anti-HA antibody) or not. Scale bar, 15 μ m. **f** Representative immunofluorescence staining for LXR α -GFP (green) and HA-ACTA2 (red, stained by anti-HA antibody) in HEK-293A cells. Scale bar, 10 μ m. **g–j** Two-color STORM images and quantification of the colocalization degree between LXR α and G-actin as well as Importin α in WT VSMCs with (**h**) or without (**g**) CytoB treatment and *Sm22a*^{-/-} VSMCs with (**i**) Ad-GFP-SM22 α infection or without (**j**) Ad-GFP-SM22 α infection ($n > 10$). **k** Co-immunoprecipitation of LXR α and Importin α , Importin β or ACTA2 in WT and *Sm22a*^{-/-} VSMCs with or without JPK, CytoB, PDGF-BB and Ad-GFP-SM22 α treatment ($n = 3$). **l** Double immunofluorescence staining for Importin α (red) and LXR α (green) in WT and *Sm22a*^{-/-} VSMCs as well as CytoB-treated WT VSMCs. Scale bar, 15 μ m. **m** Co-immunoprecipitation of LXR α and Importin α , Importin β or ACTA2 in WT VSMCs transfected with HA-ACTA2 of different concentrations ($n = 3$). Data and images represent at least three independent experiments.

phenotypes. These results were verified by immunofluorescence staining and confocal analysis (Fig. 5l). Next, we used STORM to examine the spatial relationship of LXRA to Importin α . In WT VSMCs, LXRA colocalized with Importin α , which was reflected by a nearest-neighbor distribution with a sharp peak near the 10–50 nm theoretical resolution limit of STORM (Fig. 5g), whereas disruption of F-actin by CytoB treatment or SM22 α knockout completely eliminated this natural colocalizations (Fig. 5h, i), which displayed increased dramatically the nearest-neighbor distribution. The degree of colocalization between LXRA and Importin α was similar to WT cells upon the rescue of SM22 α expression (Fig. 5j). This finding was supported by co-immunoprecipitation experiments (Fig. 5m). Taken together, these results suggest that G-actin acts as a molecular shield against LXRA binding to Importin α .

The C-terminal domain mediates the interaction between G-actin and LXRA

To characterize which part of ACTA2 is responsible for LXRA interaction, we then reconstructed the two structural domains of ACTA2 with HA-tagged truncated N-terminus (HA-ACTA2-NT, aa. 1–140) and C-terminal domains (HA-ACTA2-CTD, aa. 141–377) (Supplementary Fig. 6a), and used different truncation derivatives of ACTA2 to gain insight into the location of the interaction. The cells expressing HA-ACTA2-CTD displayed increased LXRA-GFP fluorescence intensity in the cytoplasm and reduced nuclear localization of LXRA-GFP (Fig. 6a) like HA-ACTA2-overexpressed cells (Fig. 5f). Furthermore, the ACTA2-CTD, but not ACTA2-NT, colocalized with LXRA-GFP in the cytoplasm. Similarly, in HEK293A cells co-expressing LXRA-GFP and ACTA2 truncation derivatives, the ACTA2-CTD colocalized with LXRA-GFP in the cytoplasm and abolished nuclear LXRA-GFP, whereas the ACTA2-NT did not influence the nuclear accumulation of LXRA-GFP (Fig. 6b), suggesting that ACTA2-CTD predominantly contributed to this interaction and retarded nuclear import of LXRA.

Because there were no RPEL motifs that bind to actin in LXRA sequence [38], in turn, we constructed the two truncated mutants of LXRA-N-terminus (NT, aa. 1–170) that contained the DNA binding domain and three nuclear localization sequences (NLSs) (NLS1, 2 and 4) and LXRA-C-terminal domains (CTD, aa. 171–445) that included the hinge region, one NLS (NLS3) and the putative ligand-binding domain (Supplementary Fig. 6b) [8, 39], and transfected them into *Sm22 α ^{-/-}* VSMCs. We showed that only LXRA-NT was accumulated in the nucleus, and LXRA-CTD, like endogenous LXRA, was also trapped in the cytoplasm of *Sm22 α ^{-/-}* cells (Fig. 6c). Similarly, nuclear localization of only LXRA-NT was observed in HEK293A cells co-expressing HA-ACTA2-CTD, whereas LXRA-CTD colocalized with ACTA2-CTD in the cytoplasm (Fig. 6d). Next, peptide pull-down experiments with recombinant purified GST-LXRA, GST-LXRA-NT, and GST-LXRA-CTD revealed that both GST-LXRA and GST-LXRA-CTD bound directly to ACTA2 and ACTA2-CTD rather than ACTA2-NT (Fig. 6e). Thus, LXRA-CTD is the region for ACTA2 recognizing and binding to LXRA. Together, these data suggest that the C-terminal domains mediate the interaction between G-actin and LXRA.

DISCUSSION

In the present study, we showed that the depletion of SM22 α dysregulated LXRA signaling and promoted foam cell formation of VSMCs and the development of atherosclerosis. G-actin interacted with LXRA and inhibited its nuclear import, as the complex blocked LXRA binding to Importin α . SM22 α regulated the nuclear localization of LXRA through a mechanism in which F-actin polymerization by SM22 α led to dissociation of this complex (Fig. 6f). Using *Sm22 α ^{-/-}* and *Sm22 α ^{-/-}Ldlr^{-/-}* mice, we provide evidence for a causative role of SM22 α loss in LXRA signaling and

VSMCs foam cell formation. G-actin was identified as a negative regulator of the LXRA nuclear import and activity.

The disruption of LXRA is believed to be an important factor in the pathological development of atherosclerosis via leading to foam cell formation in macrophages of the arterial wall [9, 40, 41]. Though the expression of LXRA is lower in human VSMCs, limited studies have demonstrated that LXRA can influence proliferation, contractility, apoptosis, and calcification in VSMCs [42]. Moreover, ABCA1 expression is reduced in neointimal VSMCs compared with those isolated from the medial layer [43], more so in advanced relative to early atherosclerosis [44]. In the current study, similar atherosclerotic phenotypes to those of LXRA-deficient mice were observed in *Sm22 α ^{-/-}* mice in the context of hypercholesterolemia. The diffuse thickenings of the vascular walls and aortic stiffness existed in *Sm22 α ^{-/-}* mice on a Paigen diet for 12 weeks, which are widely considered the most likely precursor of atherosclerotic plaques [1, 45]. Rescue of SM22 α expression could alleviate cholesterol overload and displayed anti-atherogenic effects that presented as reduced aortic stiffness and lesion area. Interestingly, we demonstrated that one different aspect from the study on *Lxra^{-/-}* mice is that the increased atherosclerosis in *Sm22 α ^{-/-}* mice is associated with an inability of VSMCs rather than macrophages to efficiently efflux cholesterol through the LXR pathway. More importantly, the observation that nuclear import of LXRA was impaired in VSMCs of *Sm22 α ^{-/-}* mice was removed by the rescue of SM22 α expression in vitro and in vivo. Our findings suggest a particularly important role for SM22 α in LXRA-mediated cholesterol homeostasis and contractile phenotype in VSMCs especially in the context of hypercholesterolemia and provide evidence that SM22 α contributes to the anti-atherogenic effects of LXRA on VSMCs.

De-differentiation, modulation or phenotype switching of VSMCs is characterized by reduced myofilament density and lower expression of contractile proteins [1]. It is known that modulated VSMCs predominate in the thickened arterial intima at atherosclerosis-prone sites prior to the onset of plaque formation and VSMC foam cell formation is resulted from modulated VSMCs engulfing oxidized low-density lipoprotein [46]. In the present study, the proteomic and lipidomic analysis showed that SM22 α loss correlated with reduced LXRA-ABCA1 expression and increased cholesteryl ester in phenotypically modulated VSMCs. We validated that LXRA was redistributed from the nuclear to the cytoplasm in VSMCs upon PDGF-BB stimulation and in the neointima VSMCs and that LXRA colocalized with G-actin in the cytoplasm, suggesting that LXRA nuclear localization is regulated by actin dynamics and is impaired as a result of VSMC phenotypic switching. Our findings indicated that SM22 α loss-mediated aberrant actin-LXRA signaling pathway guides modulated VSMCs to ultimately transform into foam cells. Our results support the idea that lipid metabolism programming is a critical event in phenotypic switching of VSMCs and that SM22 α activates the LXRA-ABCA1 axis to maintain lipid homeostasis through the modulation of cytoskeletal actin polymerization.

We acknowledge several limitations of this study. First, SM22 α is not only expressed in SMCs but also expressed in other lineages, such as cardiomyocytes during development and myeloid cells [47]. Therefore, using inducible SMC-specific SM22 α knockout mice are warranted to accurately define a more definitive causal relationship between SM22 α expression in VSMCs and their contribution to atherosclerotic lesion formation. Second, polymerization and depolymerization in live cells are regulated by actin-binding proteins. It needs further to explore whether and how other actin-binding proteins are involved in the regulation of LXRA signaling and cholesterol metabolism. Finally, given the involvement of the actin cytoskeleton remodeling in phenotypic switching of VSMC, it will be important to determine how these and similar pathways of aberrant actin-to-LXRA crosstalk can be intervened by the development of therapeutic agents.

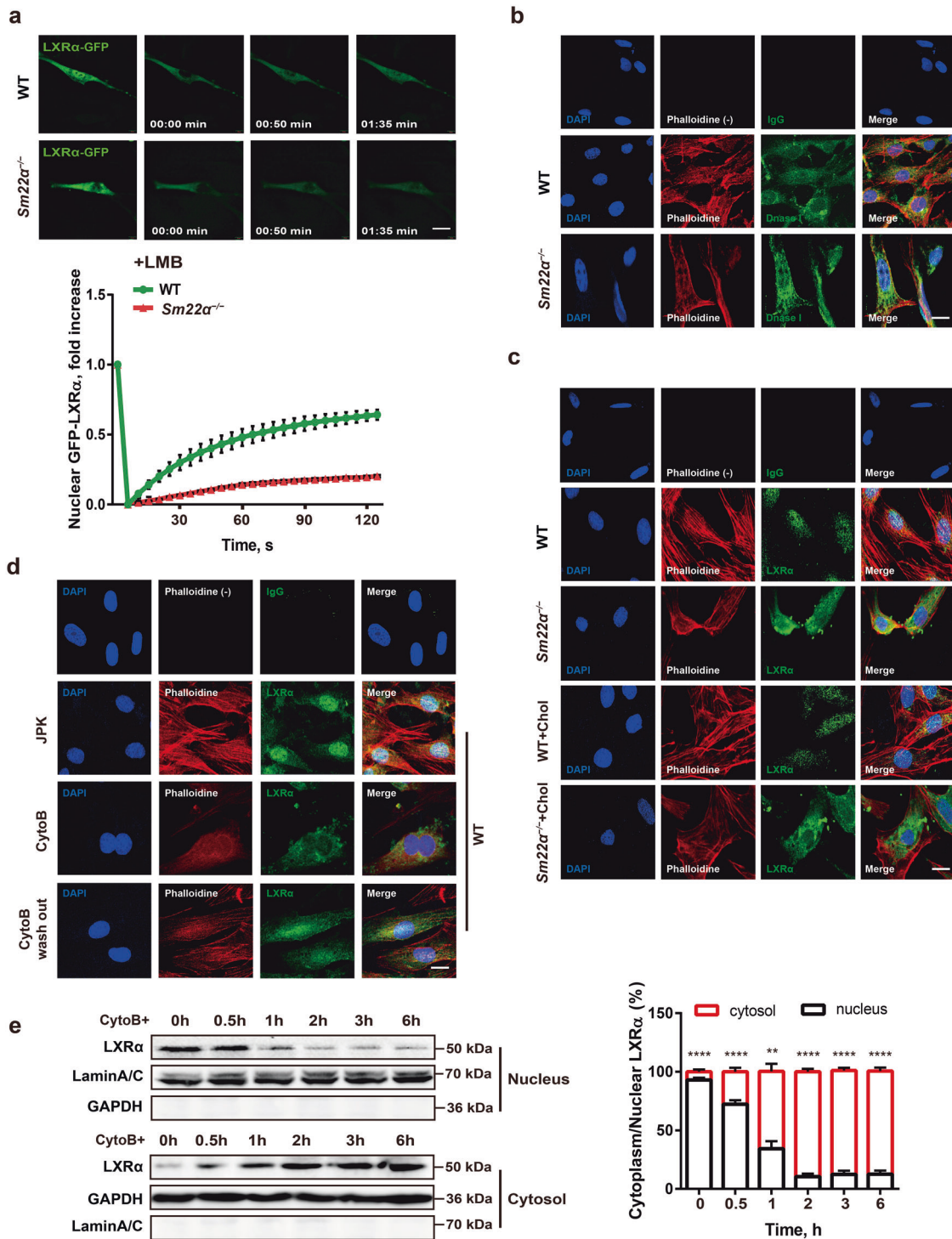


Fig. 6 The C-terminal domain mediates the interaction between G-actin and LXRα. **a** Representative immunofluorescence staining for LXRα-GFP (green) in WT VSMCs transfected with HA-ACTA2-CTD (red) or HA-ACTA2-NT (red). Scale bar, 15 μm. **b** Representative immunofluorescence staining for LXRα-GFP (green) and HA-ACTA2-CTD (red) or HA-ACTA2-NT (red) in HEK-293A cells. Scale bar, 15 μm. **c** LXRα-CTD-GFP (green) or LXRα-NT-GFP (green) was transfected into *Sm22α^{-/-}* VSMCs. Scale bar, 10 μm. **d** LXRα (-CTD, -NT)-GFP (green) and HA-ACTA2-CTD (red) were co-expressed in HEK-293A cells. Scale bar, 10 μm. **e** Interaction of HA-ACTA2 (-FL, -CTD, -NT) and GST-LXRα (-FL, -CTD, -NT) proteins analyzed by in vitro pull-down assay ($n = 3$). **f** Schematic representation of a working model in which SM22α inhibits VSMC-derived foam cell formation by blocking actin-LXRα signaling ameliorating atherosclerosis. Data and images represent at least three independent experiments.

DATA AVAILABILITY

The data that support the findings of this study are available from the corresponding author upon reasonable request.

REFERENCES

- Basatemur GL, Jrgensen HF, Clarke MCH, Bennett MR, Mallat Z. Vascular smooth muscle cells in atherosclerosis. *Nat Rev Cardiol.* 2019;16:727–44.
- Glass CK, Witztum JL. Atherosclerosis. The road ahead. *Cell.* 2001;104:503–16.
- Libby P, Ridker PM, Hansson GK. Progress and challenges in translating the biology of atherosclerosis. *Nature.* 2011;473:317–25.
- Allahverdian S, Chehroudi AC, Mcmanus BM, Abraham T, Francis GA. Contribution of intimal smooth muscle cells to cholesterol accumulation and macrophage-like cells in human atherosclerosis. *Circulation.* 2014;129:1551–9.
- Shankman LS, Gomez D, Cherepanova OA, Salmon M, Alencar GF, Haskins RM, et al. KLF4-dependent phenotypic modulation of smooth muscle cells has a key role in atherosclerotic plaque pathogenesis. *Nat Med.* 2015;21:628–37.
- Bensinger SJ, Tontonoz P. Integration of metabolism and inflammation by lipid-activated nuclear receptors. *Nature.* 2008;454:470–7.
- Ferber Dan. Possible new way to lower cholesterol. *Science.* 2000;289:1446–7.
- Prufer K, Boudreaux J. Nuclear localization of liver X receptor alpha and beta is differentially regulated. *J Cell Biochem.* 2007;100:69–85.
- Schuster GU, Parini P, Wang L, Alberti S, Steffensen KR, Hansson GK, et al. Accumulation of foam cells in liver X receptor-deficient mice. *Circulation.* 2002;106:1147–53.
- Wirka RC, Wagh D, Paik DT, Pjanic M, Nguyen T, Miller CL, et al. Atheroprotective roles of smooth muscle cell phenotypic modulation and the TCF21 disease gene as revealed by single-cell analysis. *Nat Med.* 2019;25:1280–9.
- Zhang JC, Kim S, Helmke BP, Yu WW, Du KL, Lu MM, et al. Analysis of SM22alpha-deficient mice reveals unanticipated insights into smooth muscle cell differentiation and function. *Mol Cell Biol.* 2001;21:1336–44.
- Fu Y, Liu HW, Forsythe SM, Kogut P, McConville JF, Halayko AJ, et al. Mutagenesis analysis of human SM22: characterization of actin binding. *J Appl Physiol.* 2000;89:1985–90.
- Han M, Dong LH, Zheng B, Shi JH, Wen JK, Cheng Y. Smooth muscle 22 alpha maintains the differentiated phenotype of vascular smooth muscle cells by inducing filamentous actin bundling. *Life Sci.* 2009;84:394–401.
- Wamhoff BR, Hoofnagle MH, Burns A, Sinha S, McDonald OG, Owens GK. A G/C element mediates repression of the SM22alpha promoter within phenotypically modulated smooth muscle cells in experimental atherosclerosis. *Circ Res.* 2004;95:981–8.
- Feil S, Fehrenbacher B, Lukowski R, Essmann F, Schulze-Osthoff K, Schaller M, et al. Transdifferentiation of vascular smooth muscle cells to macrophage-like cells during atherogenesis. *Circ Res.* 2014;115:662–7.
- Feil S, Hofmann F, Feil R. SM22alpha modulates vascular smooth muscle cell phenotype during atherogenesis. *Circ Res.* 2004;94:863–5.
- Shen J, Yang M, Ju D, Jiang H, Zheng JP, Xu Z, et al. Disruption of SM22 promotes inflammation after artery injury via nuclear factor kappaB activation. *Circ Res.* 2010;106:1351–62.
- Shu YN, Zhang F, Bi W, Dong LH, Zhang DD, Chen R, et al. SM22a inhibits vascular inflammation via stabilization of Ikbeta in vascular smooth muscle cells. *J Mol Cell Cardiol.* 2015;84:191–9.
- Shu YN, Dong LH, Li H, Pei QQ, Miao SB, Zhang F, et al. CKII-SIRT1-SM22a loop evokes a self-limited inflammatory response in vascular smooth muscle cells. *Cardiovasc Res.* 2017;113:1198–207.
- Dong LH, Wen JK, Liu G, McNutt MA, Miao SB, Gao R, et al. Blockade of the Ras-extracellular signal-regulated kinase 1/2 pathway is involved in smooth muscle 22 alpha-mediated suppression of vascular smooth muscle cell proliferation and neointima hyperplasia. *Arterioscler Thromb Vasc Biol.* 2010;30:683–91.
- Zhong L, He X, Si X, Wang H, Li B, Hu Y, et al. SM22a (smooth muscle 22a) prevents aortic aneurysm formation by inhibiting smooth muscle cell phenotypic switching through suppressing reactive oxygen species/NF-kB (nuclear factor-kB). *Arterioscler Thromb Vasc Biol.* 2019;39:10–25.
- Lv P, Miao SB, Shu YN, Dong LH, Liu G, Xie XL, et al. Phosphorylation of smooth muscle 22a facilitates angiotensin II-induced ROS production via activation of the PKCδ-P47phox axis through release of PKCδ and actin dynamics and is associated with hypertrophy and hyperplasia of vascular smooth muscle cells in vitro and in vivo. *Circ Res.* 2012;111:697–707.
- Chen R, Zhang F, Song L, Shu Y, Lin Y, Dong L, et al. Transcriptome profiling reveals that the SM22a-regulated molecular pathways contribute to vascular pathology. *J Mol Cell Cardiol.* 2014;72:263–72.
- Cavalcante JL, Lima JA, Redheuil A, Al-Mallah MH. Aortic stiffness: current understanding and future directions. *J Am Coll Cardiol.* 2011;57:1511–22.
- Lv P, Yin YJ, Kong P, Cao L, Xi H, Wang N, et al. SM22alpha loss contributes to apoptosis of vascular smooth muscle cells via macrophage-derived circRasGEF1B. *Oxid Med Cell Longev.* 2021;2021:5564884.
- Whitney KD, Watson MA, Goodwin B, Galardi CM, Maglich JM, Wilson JG, et al. Liver X receptor (LXR) regulation of the LXRalpha gene in human macrophages. *J Biol Chem.* 2001;276:43509–15.
- Beaven SW, Wroblewski K, Wang J, Hong C, Bensinger S, Tsukamoto H, et al. Liver X receptor signaling is a determinant of stellate cell activation and susceptibility to fibrotic liver disease. *Gastroenterology.* 2011;140:1052–62.
- Hamilton JP, Koganti L, Muchenditsi A, Pendyala VS, Huso D, Hankin J, et al. Activation of liver X receptor/retinoid X receptor pathway ameliorates liver disease in Atp7B(-/-) (Wilson disease) mice. *Hepatology.* 2016;63:1828–41.
- Owens GK, Kumar MS, Wamhoff BR. Molecular regulation of vascular smooth muscle cell differentiation in development and disease. *Physiol Rev.* 2004;84:767–801.
- Sanyour HJ, Li N, Rickel AP. Statin-mediated cholesterol depletion exerts coordinated effects on the alterations in rat vascular smooth muscle cell biomechanics and migration. *J Physiol.* 2020;598:1505–1522.
- Wu S, Yin R, Ernest R, Li Y, Zhelyabovska O, Luo J, et al. Liver X receptors are negative regulators of cardiac hypertrophy via suppressing NF-kB signalling. *Cardiovasc Res.* 2009;84:119–26.
- Rochette-Egly C. Nuclear receptors: integration of multiple signalling pathways through phosphorylation. *Cell Signal.* 2003;15:355–66.
- Calkin AC, Tontonoz P. Transcriptional integration of metabolism by the nuclear sterol-activated receptors LXR and FXR. *Nat Rev Mol Cell Biol.* 2012;13:213–24.
- Saha T, Guha D, Manna A, Panda AK, Bhat J, Chatterjee S, et al. G-actin guides p53 nuclear transport: potential contribution of monomeric actin in altered localization of mutant p53. *Sci Rep.* 2016;6:32626.
- Ho CY, Jaalouk DE, Vartiainen MK, Lammerding J. Lamin A/C and emerin regulate MKL1-SRF activity by modulating actin dynamics. *Nature.* 2013;497:507–11.
- Zhou R, Han B, Xia C. Membrane-associated periodic skeleton is a signaling platform for RTK transactivation in neurons. *Science.* 2019;365:929–34.
- Goldfarb DS, Corbett AH, Mason DA, Harreman MT, Adam SA. Importin alpha: a multipurpose nuclear-transport receptor. *Trends Cell Biol.* 2004;14:505–14.
- Miralles F, Posern G, Zaromytidou AI, Treisman R. Actin dynamics control SRF activity by regulation of its coactivator MAL. *Cell.* 2003;113:329–42.
- Li X, Zhang S, Blander G, Tse JG, Krieger M, Guarente L. SIRT1 deacetylates and positively regulates the nuclear receptor LXR. *Mol Cell.* 2007;28:91–106.
- Tangirala RK, Bischoff ED, Joseph SB, Wagner BL, Walczak R, Laffitte BA, et al. Identification of macrophage liver X receptors as inhibitors of atherosclerosis. *Proc Natl Acad Sci USA.* 2002;99:11896–901.
- Joseph SB, Castrillo A, Laffitte BA, Mangelsdorf DJ, Tontonoz P. Reciprocal regulation of inflammation and lipid metabolism by liver X receptors. *Nat Med.* 2003;9:213–9.
- Calkin AC, Tontonoz P. Liver x receptor signaling pathways and atherosclerosis. *Arterioscler Thromb Vasc Biol.* 2010;30:1513–8.
- Choi HY, Rahmani M, Wong BW, Allahverdian S, McManus BM, Pickering JG, et al. ATP-binding cassette transporter A1 expression and apolipoprotein A-I binding are impaired in intima-type arterial smooth muscle cells. *Circulation.* 2009;119:3223–31.
- Bradley MN, Hong C, Chen M, Joseph SB, Wilpitz DC, Wang X, et al. Ligand activation of LXR beta reverses atherosclerosis and cellular cholesterol overload in mice lacking LXR alpha and apoE. *J Clin Invest.* 2007;117:2337–46.
- Virmani R, Kolodgie FD, Burke AP, Farb A, Schwartz SM. Lessons from sudden coronary death: a comprehensive morphological classification scheme for atherosclerotic lesions. *Arterioscler Thromb Vasc Biol.* 2000;20:1262–75.
- Vengrenyuk Y, Nishi H, Long X, Ouimet M, Savji N, Martinez FO, et al. Cholesterol loading reprograms the microRNA-143/145-myocardin axis to convert aortic smooth muscle cells to a dysfunctional macrophage-like phenotype. *Arterioscler Thromb Vasc Biol.* 2015;35:535–46.
- Raja C, Fatima ZS, Ana CC, Diane SK, Daniel MG, Kathleen AM. Promoters to study vascular smooth muscle: mistaken identity? *Arterioscler Thromb Vasc Biol.* 2019;39:603–12.

ACKNOWLEDGEMENTS

We thank Dr. Mingming Gao at Lipid Metabolism Laboratory for technical support on animal experiments; Dr. Chang Wang and Huan Chen at Human Anatomy Department for technical support with FLIP and FRAP experiments; Dr. Ce Liang at Pharmacology Department for technical support with STORM experiments; Dr. Hongyuan Yang at School of Biotechnology and Biomolecular Sciences of Australia University of New South Wales for discussions, and comments on the data.

AUTHOR CONTRIBUTIONS

MH initiated the project and designed the paper. D-DZ, YS, and PK performed most of the experiments and/or analyzed data. Y-KG, XX, X-WW, and Y-LL assisted in animal experiments. LW, Y-QD, and FZ assisted in in vitro experiments and histological analyses. PK and D-DZ generated the illustrations. MH wrote the manuscript and edited the manuscript. All authors read and approved the final manuscript.

FUNDING

This work was supported by the National Natural Science Foundation of China, including 91739301, 91849102, and 31872788. This work was funded by the Key Natural Science Foundation Projects of Hebei Province H2019206028, Natural Science Foundation of Hebei Province H2021206006 and H2021423047, and Natural Science Youth Fund of Hebei Province Education Department QN2020167, by the administrative departments of science and technology at the Hebei Medical University with funding from the Project Supporting Fund established and appropriated by the Hebei Medical University Budget Committee.

COMPETING INTERESTS

The authors declare no competing interests.

ADDITIONAL INFORMATION

Supplementary information The online version contains supplementary material available at <https://doi.org/10.1038/s41419-021-04239-w>.

Correspondence and requests for materials should be addressed to Mei Han.

Reprints and permission information is available at <http://www.nature.com/reprints>

Publisher's note Springer Nature remains neutral with regard to jurisdictional claims in published maps and institutional affiliations.



Open Access This article is licensed under a Creative Commons Attribution 4.0 International License, which permits use, sharing, adaptation, distribution and reproduction in any medium or format, as long as you give appropriate credit to the original author(s) and the source, provide a link to the Creative Commons license, and indicate if changes were made. The images or other third party material in this article are included in the article's Creative Commons license, unless indicated otherwise in a credit line to the material. If material is not included in the article's Creative Commons license and your intended use is not permitted by statutory regulation or exceeds the permitted use, you will need to obtain permission directly from the copyright holder. To view a copy of this license, visit <http://creativecommons.org/licenses/by/4.0/>.

© The Author(s) 2021